

Nanoscale

Accepted Manuscript



This is an *Accepted Manuscript*, which has been through the Royal Society of Chemistry peer review process and has been accepted for publication.

Accepted Manuscripts are published online shortly after acceptance, before technical editing, formatting and proof reading. Using this free service, authors can make their results available to the community, in citable form, before we publish the edited article. We will replace this *Accepted Manuscript* with the edited and formatted *Advance Article* as soon as it is available.

You can find more information about *Accepted Manuscripts* in the [Information for Authors](#).

Please note that technical editing may introduce minor changes to the text and/or graphics, which may alter content. The journal's standard [Terms & Conditions](#) and the [Ethical guidelines](#) still apply. In no event shall the Royal Society of Chemistry be held responsible for any errors or omissions in this *Accepted Manuscript* or any consequences arising from the use of any information it contains.

ARTICLE

Charge Separation in Facet Engineered Chalcogenide Photocatalyst: A Selective Photocorrosion Approach

Cite this: DOI: 10.1039/x0xx00000x

Naixu Li,^{a†} Maochang Liu,^{b†} Zhaohui Zhou,^{b†} Jiancheng Zhou,^{a,*} Yueming Sun,^a and Liejin Guo^{b,*}

Received 00th January 2012,

Accepted 00th January 2012

DOI: 10.1039/x0xx00000x

www.rsc.org/

Finding of active sites for photocatalytic reduction and oxidation allows the mechanistic understanding towards a given reaction, ensuring the rational design and fabrication of an efficient photocatalyst. Herein, using well-shaped Cu_2WS_4 decahedra as model photocatalysts, we demonstrated that photoinduced oxidative etching could be taken as an indication to the photooxidation reaction sites of chalcogenide photocatalyst as it only occurred on {101} facets of Cu_2WS_4 during photocatalytic hydrogen production. The photocatalytic reduction reaction, in contrast, was confined on its {001} facets. Based on this finding, the photocatalytic activity of Cu_2WS_4 decahedra could be further tailored by controlling the ratio of {001}/{101} facets. This work thus provides a general route to the determination of reactive sites on shaped chalcogenide photocatalysts.

Introduction

Semiconductor-based solar hydrogen production has been widely accepted as a potential alternative for the future addressing the unprecedented increases of world energy and environment demands.^[1] Although the emergence of the concept can be traced back to the groundbreaking work on the photo-electrochemical water splitting over Pt/TiO₂ electrodes by Fujishima and Honda in 1972, only within the last decade have great advances become available on the photocatalytic activity and stability.^[2] Various kinds of photocatalysts, including sulfides, oxides, nitrides, metallic oxides, and their combinations have been successfully developed.^[3] Yet, there is still a far way in approaching the industrial application.

Generally, upon excitation by light irradiation, there are two choices for the generated e^-/h^+ pairs: *i*) migrated and separated on the surface of the semiconductor crystal to trigger reduction/oxidation reactions; *ii*) recombined in the bulk before arriving at the surface of the semiconductor crystals, which is highly undesired.^[1b, 1g] One of the keys to improving the photocatalytic activity is the successful design of semiconductor-based architectures with effective charge separation.^[3c, 4] In fact, the fate of photogenerated e^-/h^+ highly relies on the surface structure of the given photocatalyst.^[5] Recently, studies have been carried out on well-shaped single-crystal oxide, like TiO₂ and BiVO₄. Both experimental and computational studies suggested separated photoinduced reduction and oxidation sites on different facets, and thereby enhanced charge separation.^[5d, 6] For anatase TiO₂ single crystal, {001} facets were found to be active for an oxidation

reaction, while {101} facets were responsible for a reduction reaction.^[5d, 6b, 6c] Li *et al.* also reported that photoexcited e^-/h^+ could be effectively separated on {010} and {110} facets of monoclinic BiVO₄ single crystals.^[5a] Fundamentally, the successes are based on the observation of spatial separation of photogenerated charges over different crystal facets of the semiconductors with an in-situ photoreduction/oxidation procedure.^[5a, 5d, 5g] For example, to determine the site of photoinduced oxidation reaction, soluble Mn(II) or Pb(II) precursors (typically in the form of Mn(NO₃)₂ and Pb(NO₃)₂) as sacrificial reagents should be used with MnO₂ or PdO₂ selectively deposited on the certain crystal facets. However, it could become a failure when the photocatalysts are sulfides as the Mn(II) or Pb(II) salts can react with S²⁻ from the photocatalyst. This will essentially destroy the surface structures of the photocatalyst without indicating the oxidation reaction sites. Consequently, it is highly valued to extend the method as well as develop novel methods to narrow-band-gap based chalcogenide photocatalysts, which usually exhibit much higher photocatalytic activity towards solar hydrogen production.

Herein, with the use of decahedral Cu_2WS_4 single crystals as a model chalcogenide photocatalyst, we reported that photoinduced oxidative etching, which is known to be detrimental to the integrity of semiconductor crystal surface and suggested to be avoided, could be used to determine the reaction site of photocatalytic oxidation on the surface of chalcogenide photocatalysts. Furthermore, we successfully demonstrated that energy-driven vectorial charge transfer could be reached between adjacent {001} and {101} facets.

Our results therefore provide a novel approach to studying crystal-facet engineered charge separation over shaped chalcogenide photocatalysts during the photocatalytic process.

Experimental Section

Chemicals and Materials. Cuprous chloride (CuCl), sodium tungstate dihydrate ($\text{Na}_2\text{WO}_4 \cdot 2\text{H}_2\text{O}$), thioacetamide (CH_3CSNH_2), ammonium hexachloroplatinate ($(\text{NH}_4)_2\text{PtCl}_6$), ammonium hexachlororuthenate ($(\text{NH}_4)_2\text{RuCl}_6$), manganese (II) nitrate ($\text{Mn}(\text{NO}_3)_2$, 50 % solution), lead (II) nitrate ($\text{Pb}(\text{NO}_3)_2$), sodium sulfide (Na_2S), sodium sulfite (Na_2SO_3), ethanol ($\text{CH}_3\text{CH}_2\text{OH}$), and polyvinyl pyrrolidone (PVP, MW $\approx 55,000$) were used as received. The water used in all syntheses was de-ionized water with a resistivity of 18.2 $\text{M}\Omega\cdot\text{cm}$.

Synthesis of Cu_2WS_4 decahedra. Cu_2WS_4 was prepared by hydrothermal synthesis. In a typical process: $\text{Na}_2\text{WO}_4 \cdot 2\text{H}_2\text{O}$ (0.005 mol), CuCl (0.01 mol) and thioacetamide (0.025 mol) were added to the solution containing deionized water (30 mL) and ethanol (30 ml) with magnetic stirring to form a homogeneous suspension. The reaction mixture was then sealed in a 100 mL capacity teflon-lined stainless steel autoclave. The sealed mixture was heated at 200 °C for 72 h. After cooling, the product was separated by centrifugation, washed with deionized water and ethanol several times, and dried at 80 °C for 4 h in a vacuum oven. Cu_2WS_4 decahedra prepared in this standard process were found with moderate percentage of {001} facets (See Figure 1). If we add 1.11 g of PVP into the standard reaction, we can obtain Cu_2WS_4 decahedra with large {001} surface coverage (see Main Text, Figure 8C). If we use deionized water (20 mL) and ethanol (20 ml) in the standard synthesis, the obtained Cu_2WS_4 decahedra will be with small coverage of {001} facets (see Main Text, Figure 8A).

In-situ synthesis of Pt/ Cu_2WS_4 photocatalyst. Typically, the as-prepared Cu_2WS_4 was dispersed by a magnetic stirrer in an aqueous (180 mL) containing Na_2S (0.35 M) and Na_2SO_3 (0.25 M), a certain amount of $(\text{NH}_4)_2\text{PtCl}_6$ with 0.5 wt% or 5 wt% Pt/catalyst was then added into solution. The obtained suspension was irradiated by Xe lamp for several hours. After reaction, the product was separated by centrifugation, washed with deionized water several times, and dried at 80 °C for 4 h in a vacuum oven.

Synthesis of Ru/ Cu_2WS_4 , MnS/ Cu_2WS_4 , PbS/ Cu_2WS_4 photocatalysts. The process is similar to the synthesis of Pt/ Cu_2WS_4 photocatalyst except using $(\text{NH}_4)_2\text{RuCl}_6$, $\text{Mn}(\text{NO}_3)_2$ (50% solution), or $\text{Pb}(\text{NO}_3)_2$ instead of $(\text{NH}_4)_2\text{PtCl}_6$.

Synthesis of Pt- Cu_2WS_4 photocatalyst without light irradiation. The process is similar to the synthesis of Pt/ Cu_2WS_4 photocatalyst except adding 100 mg ascorbic acid as reductant, and without light irradiation.

Photocatalytic reactions. Photocatalytic reactions of hydrogen production from water were conducted in a gas-closed system with a side irradiation Pyrex cell (using CHF-XM500 Xe lamp irradiation) at 35 °C. The photocatalyst powder (0.2 g) was dispersed by a magnetic stirrer in an aqueous (180 mL) containing Na_2S (0.35 M) and Na_2SO_3 (0.25 M) as hole scavengers. The photocatalysts were irradiated with visible light through a cutoff filter ($\lambda \geq 430$ nm) from the Xe lamp. The intensity and number of photons of the two light sources were measured by a fiber optic spectrometer. The amount of H_2 gas was determined using online thermal conductivity detector (TCD) gas chromatography (NaX zeolite column, TCD detector, N_2 carrier) or drainage. Blank experiments showed that no H_2 was produced, indicating the reaction catalytically proceeded.

Computational modeling. The electronic structures of {001} and {101} surfaces of $I\text{-Cu}_2\text{WS}_4$ were studied by quantum chemical calculation, within density functional theory formalism. All calculations were performed using Vienna ab initio simulation package (VASP). An energy cutoff of 300 eV and K-points meshes of $9 \times 9 \times 1$ and $5 \times 9 \times 1$ were used for geometry optimization of {001} and {101} surfaces. The optimization was carried out until the force on each atom became < 0.02 eV/Å. The surfaces, *i.e.*, {001} and {101} facets, were constructed from an optimized unit cell of $I\text{-Cu}_2\text{WS}_4$. The surfaces were converted into a three-dimensional periodic structure by adding 20 Å vacuum slab. The width of the slab was ~ 25 Å and 13 Å for {001} and {101} surfaces, respectively. The band structure and partial density of states of both surfaces were calculated and compared for analysis.

Instrumentation. X-ray diffraction (XRD) patterns of prepared photocatalysts were confirmed by an X'Pert PRO diffractometer using Cu K α ($\lambda = 0.1538$ nm) irradiation with constant instrument parameter. And all the samples were scanned between 10 ° and 90 ° with a step size of 0.033 °. Diffuse reflectance ultraviolet-vis (UV-vis) spectra were measured on a Hitachi U-4100 spectrometer, equipped with a lab-sphere diffuse reflectance accessory. The crystallite morphologic micrographs were observed by JEOL JSM-7800F field emission scanning electron microscopy (SEM) and FEI Tecnai G2 F30 transmission electron microscope (TEM). The selected-area electron diffraction (SAED) was also performed on FEI Tecnai G2 F30 TEM. The X-ray photoelectron spectroscopy (XPS) measurements were conducted on an Axis Ultra, Kratos (UK) multifunctional spectrometer using monochromatic Al K α radiation.

Results and Discussion

Generally, the use of starting semiconductor crystals with a well-defined shape enclosed by specific facets allows us to precisely track the photocatalytic process by analyzing the shape of the products obtained after the reaction. On the other hand, element in metastable state, *e.g.*, Cu(I), as a component

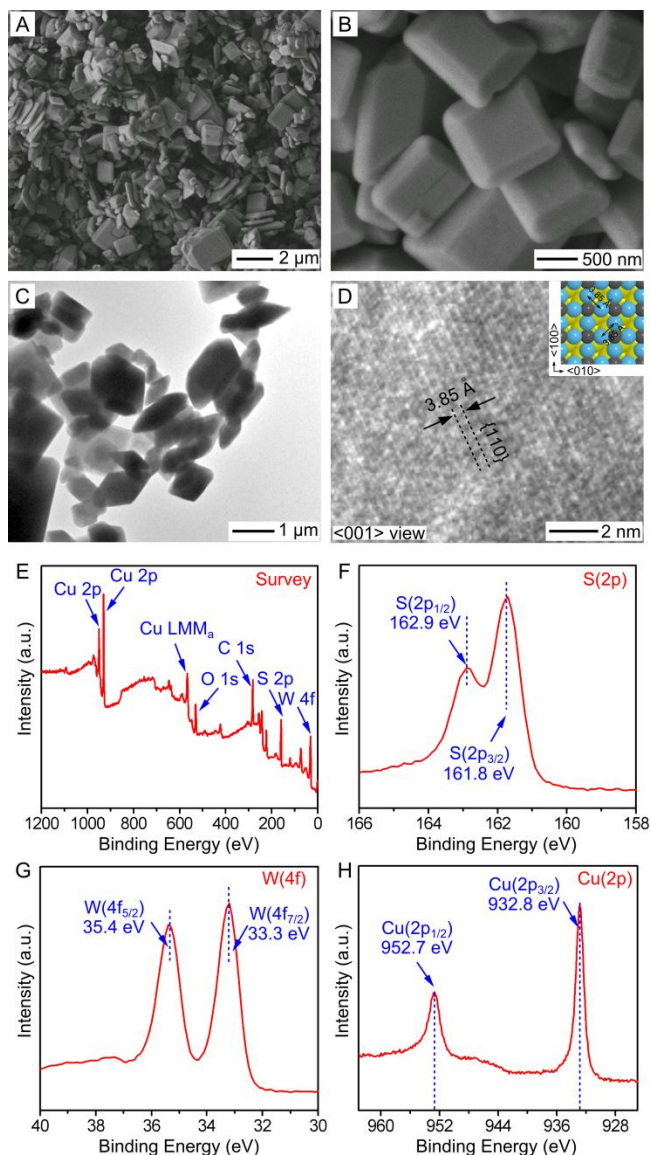


Figure 1. Cu_2WS_4 decahedra prepared using a standard procedure. A,B) SEM, C) TEM, and D) high-resolution TEM images of Cu_2WS_4 photocatalysts. E-H) XPS analysis of the Cu_2WS_4 photocatalyst with E) survey, high resolution XPS spectra of F) S, G) W, and H) Cu. Inset in (D) shows the atomic model view from [001] direction. Scale bars in (A-D) are 2 μm , 500 nm, 1 μm , and 2 nm, respectively.

of the photocatalyst, enables rapid evaluation on stability associated photocatalytic behavior. To this end, *I*- Cu_2WS_4 decahedra enclosed by {001} and {101} facets, which have been reported in one of our recent studies (and also see Figures 1 and S1 for detailed characterization), were then employed as the model chalcogenide photocatalysts.^[7] The exposed facets were further confirmed by SAED pattern viewed from [010] direction of a single-crystal Cu_2WS_4 decahedron (Figure S2). The peaks centered at 162.9/161.8 eV, 35.4/33.3 eV, and 952.7/932.8 eV shown in Figures 1F-H are typical binding energies for S, W, and Cu in their valence

states of -2, +6, and +1, respectively. In addition, the symmetric shapes of all peaks for the three elements also imply a well-structured crystal surface of Cu_2WS_4 .

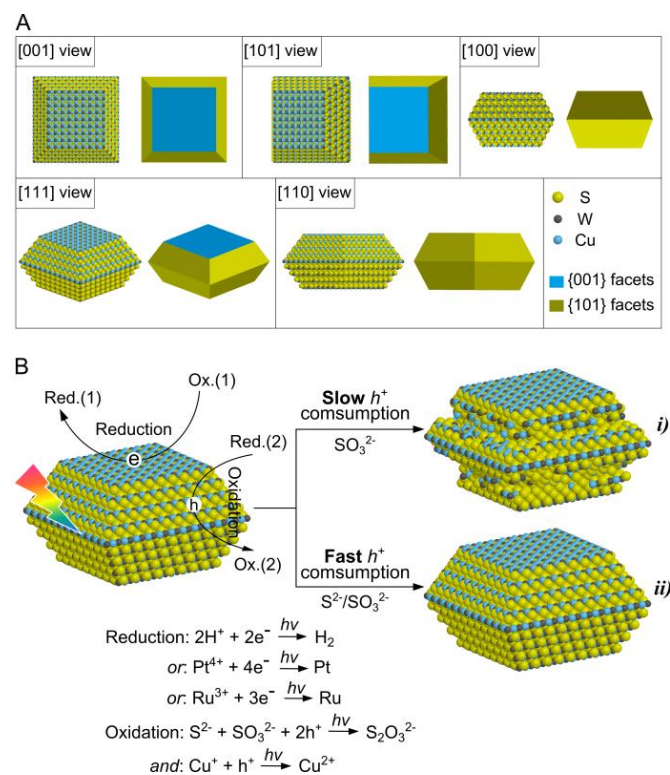


Figure 2. Effect of photoinduced oxidation reaction on the morphologic transition pattern of a Cu_2WS_4 decahedron in Na_2SO_3 or $\text{Na}_2\text{S}/\text{Na}_2\text{SO}_3$ solution. A) Atomic and 3-dimension models of a single Cu_2WS_4 decahedron. B) Atomic models for the shape evolutions of Cu_2WS_4 decahedra after the photo-reaction using Na_2SO_3 and $\text{Na}_2\text{S}/\text{Na}_2\text{SO}_3$ as sacrificial reagents, respectively.

Basically, *I*- Cu_2WS_4 is fabricated by Cu- S_4 and W- S_4 tetrahedral units. Figure 2A shows the atomic and corresponding 3-dimension models of a Cu_2WS_4 decahedron viewed from [001], [101], [100], [111], and [110] directions. It is obvious that both {001} and {101} surface showed significant deviations from their counterparts inside the crystal, containing broken Cu- S_4 or W- S_4 tetrahedrons. In particular, the change on surface atom configuration at different crystals facets will impact the electronic structures of these surfaces, leading to a unique charge-transfer behavior at the conjunctions of {001} and {101} facets.^[5a, 8] The conjecture was further evidenced by a first-principle density functional theory (DFT) calculation on the electronic structures of {001} and {101} facets. Partial density of states (DOS) over single-element contribution (Figure S3) showed that valence band (VB) at the shallow level (near the band gap) was mostly composed of S 3p and Cu 3d orbitals, whereas S 3p, W 5d, Cu 3d orbitals constituted the conduction band (CB). Taken together, the total DOS plots over the {001} and {101} facets were generated in Figure 3A. Despite the similar shape of the DOS curves, many tiny discrepancies including

ARTICLE

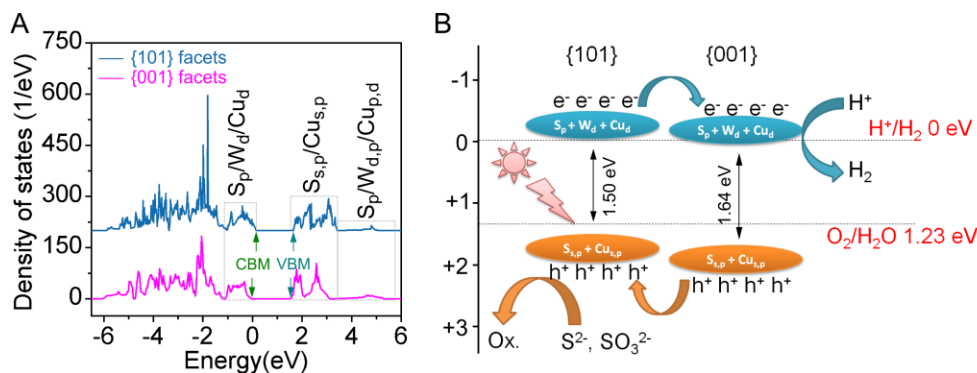


Figure 3. Calculated band structure of Cu_2WS_4 decahedron. A) Total DOS of {100} and {101} facets, and B) the corresponding energy levels.

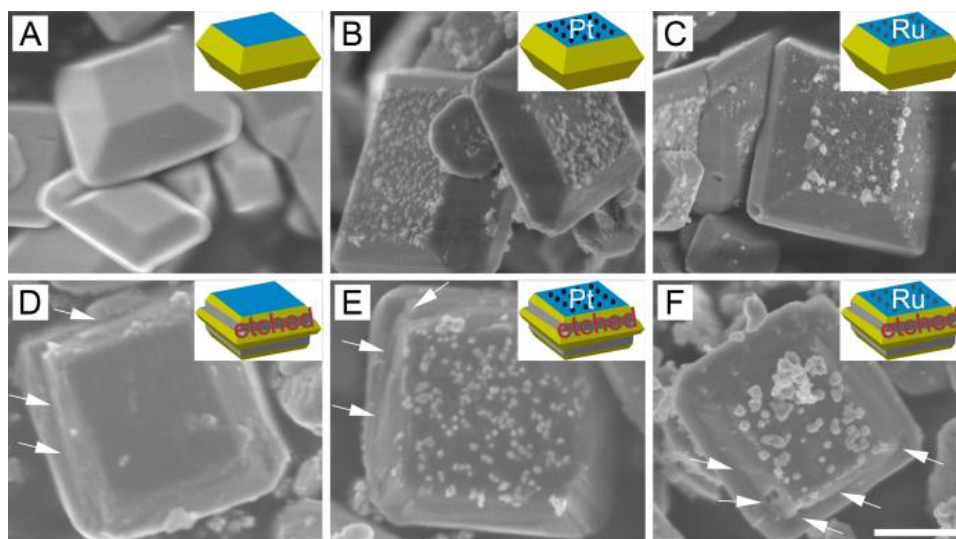


Figure 4. Surface charge separation on {100} and {101} facets revealed by introducing photoinduced oxidative etching and Pt/Ru as indications for oxidation and reduction reactions, respectively. A-C), TEM images of the recovered Cu_2WS_4 , 5 wt% Pt/ Cu_2WS_4 , and 5 wt% Ru/ Cu_2WS_4 photocatalysts after hydrogen evolution reaction for 5 h with $\text{Na}_2\text{S}/\text{Na}_2\text{SO}_3$ as sacrificial agents, and D-F), with only Na_2SO_3 as sacrificial agents. Arrows in (D-F) indicate the etched {101} facets. Insets are corresponding 3-dimension models. Scale bar in (F) is 500 nm and can be applied to (A-E).

the valence band maximum (VBM) and conduction band minimum (CBM) between the {001} and {101} facets were noticed. Although the calculation was conducted on isolated {001} and {101} facets, the already existed energy differences of them caused by the surface formation will do make charge separation available once these facets are coupled on a single crystal.^[5a, 5d, 8a] The corresponding band alignment of {001} and {101} facets was schematically shown in Figure 3B. The obtained band offsets of CB and VB

are *ca.* 80 meV and 60 meV for {001} facets relative to {101} facets, respectively, indicating the formation of type-II staggered band alignment around the connection of the two kinds of facets. According to many reported results on TiO_2 and BiVO_4 photocatalyst, it is reasonable to expect vectorial transfer of photogenerated electrons from {101} to {001}, or vice versa for photogenerated holes.^[5a, 8]

Typically, photocatalytic hydrogen production over chalcogenide semiconductors should be carried out in the

presence of sacrificial agent, usually in the form of S^{2-} or S^{2-}/SO_3^{2-} . Figure 2B schematically illustrates the photocatalytic process over the decahedral Cu_2WS_4 single crystals in the presence of SO_3^{2-} or S^{2-}/SO_3^{2-} . We assume that, upon visible-light irradiation, photogenerated electron migrates to the {001} surfaces and participates in the reduction reaction. The process can be certified by in-situ loading noble metal nanoparticles, such as Pt and Ru.^[3d, 5a] The holes, in contrast, can move to the {101} facets, leading to an oxidation of S^{2-} into S^0 . Notably, without S^{2-} (sacrificial agent only in the form of SO_3^{2-}), the holes accumulated at {001} facets will be consumed slowly. As a result, S^{2-} and Cu^+ from $Cu-S_4$ tetrahedrons of {101} facets may be oxidized and thus etched by the concentrated positive charges, leading to a collapse of the {101} surface. In other words, {101} facets will gradually tend to be rough (Figure 2B, situation *i*). If the photocatalytic reaction conducted in the presence of S^{2-}/SO_3^{2-} , the excited holes will be quickly consumed by surface absorbed S^{2-} ions from the solution, avoiding the oxidative etching of Cu_2WS_4 itself. In this case, smooth {101} facets could be maintained without subjecting surface corrosion (Figure 2B, situation *ii*).

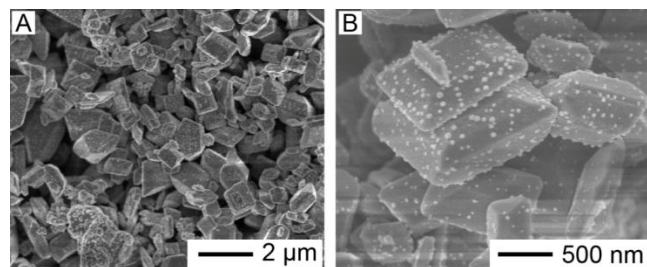


Figure 5. A) SEM and B) magnified SEM images of 5 wt% Pt- Cu_2WS_4 photocatalyst with Pt reduced by ascorbic acid and without light irradiation. The uniform distribution of Pt nanoparticles on both {001} and {101} facets indicates the non-facet selectivity of the deposition.

We then carried out a series of experiments according to the above rationales. The photocatalytic behavior was investigated with or without adding Na_2S , allowing us to in-situ check the oxidation reactions easily, and thereby the corresponding reactive sites. In a standard photocatalytic reaction, we mixed a suspension of Cu_2WS_4 decahedra (serving as the photocatalysts) with Na_2SO_3 (0.25 M) or Na_2S (0.35 M)/ Na_2SO_3 (0.25 M) as a sacrificial agent in water (as both solvent and oxidant), together with an irradiation from a 350 W Xe lamp (coupled with a 430-nm cutoff filter). Figure 4 shows SEM images of the obtained Cu_2WS_4 single crystals after a 5-hour photocatalytic reaction. Figure 4A represents the resultants with Na_2S/Na_2SO_3 as sacrificial agent. Clearly, no notable changes were observed, indicating the well maintained surface structures of the decahedra. Noble-metal precursors, *e.g.*, $(NH_4)_2PtCl_6$, $(NH_4)_3RuCl_6$, can be photoreduced into their metallic species onto the surface of semiconductor crystals and further serve as electron captures.^[7, 9] In other words, by in-situ photoreduction of

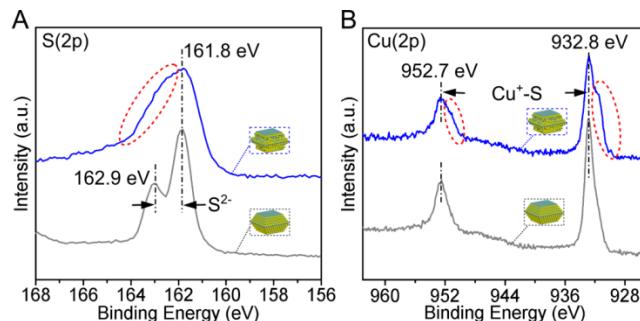


Figure 6. Comparative study on the XPS spectra of A) S 2p and B) Cu 2p over the shape-maintained Cu_2WS_4 decahedral photocatalyst (gray line) and the etched one (green line) after the reaction. Red dashed circles indicate the surface chemical states of the elements were changed over the etched sample.

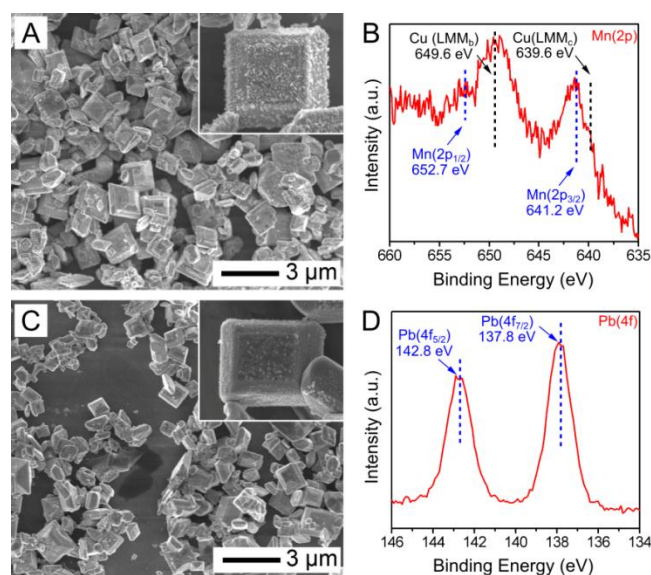


Figure 7. SEM and XPS images of as-prepared A,B) 5 wt% MnS/Cu_2WS_4 , and C,D) 5 wt% PbS/Cu_2WS_4 nanostructures. Clearly, different from what they have performed in oxide photocatalysts, $xMn(II)$ and $Pb(II)$ precursors cannot be employed to determine the oxidation reaction sites in chalcogenide photocatalysts.

noble metals, one can track the photoreduction sites by analyzing the region where the metals are deposited.^[5a, 5d, 5g] As shown in Figure 4, B and C, metallic Pt and Ru, as also validated by X-ray photoelectron spectroscopy (XPS) analysis (Figure S4), were mostly deposited on the {001} facets. Particularly, our designed experiment by direct chemical reduction, with the observation of deposition of Pt on both {001} and {101} facets in a non-irradiated reaction (Figure 5), indicated that the selective photoreduction of the noble metals was independent on the chemical difference, such as adsorption/desorption behaviors of reactant additives, atom coordinations, between the two kinds of facets.^[5a, 5g, 10] Nevertheless, when these reactions were carried out in the absence of Na_2S , namely with only Na_2SO_3 as sacrificial

reagent, similar phenomena were observed on {001} facets, however, significant corruptions arising from photooxidative etching were also noticed on the {101} facets. By further studying the XPS analysis of the recovered products in Figure 4A and 4D, slight changes on S 2p and Cu 2p scans, as expected, were only observed on the etched sample (Figure 6), reflecting the oxidation-induced variation on surface elemental chemical states.^[11] We also checked the use of soluble Mn (II) and Pb (II) as sacrificial reagents. As expected, both Mn (II) and Pb (II) were homogeneously deposited on the entire surfaces of the decahedra in the form of MnS or PbS (Figure 7) without showing the photoinduced oxidation sites, confirming our prediction.

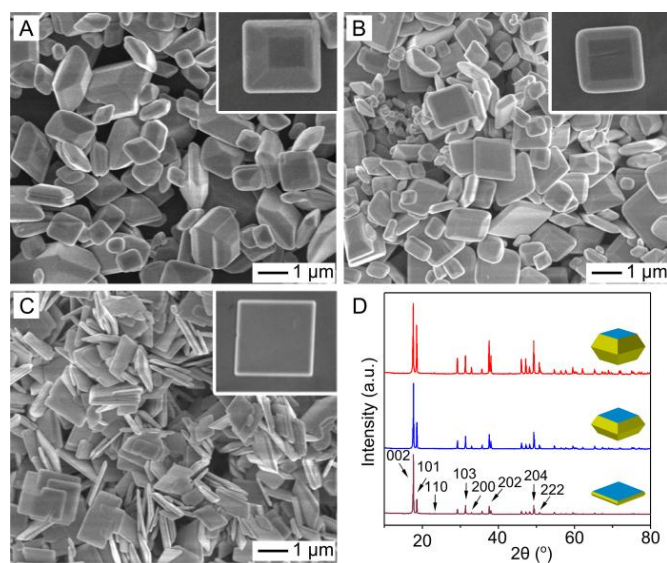


Figure 8. Morphology and crystal structure of Cu_2WS_4 decahedra prepared by different methods. A-C) SEM images of the Cu_2WS_4 decahedra with (A) small, (B) moderate, and (C) large {001} surface. D) Corresponding XRD patterns of Cu_2WS_4 decahedral photocatalysts with different ratios of {001} and {101} facets. We again include Cu_2WS_4 decahedra prepared by a standard synthesis (with moderate {001}-facet coverage) as a reference.

The above experimental results clearly validated our hypothesis shown in Figure 2B. Specifically, {001} facets provided the sites for reduction, while the photoetched {101} surface is a clear indication of oxidation active sites. It is believed that the activity of photocatalytic H_2 production undergoes a kinetic control with a determining reaction step, *i.e.*, reduction or oxidation. Regulation on the corresponding reactive sites therefore offers a versatile way of the understanding of the reaction kinetics.^[5e, 12] To this end, Cu_2WS_4 photocatalysts enclosed with controlled {001} and {101} facets were prepared with similar method. Figure 8A-C shows the representative SEM images of the decahedra with smaller (Figure 8A), moderate (Figure 8B, standard synthesis) and larger (Figure 8C) {001}-facet coverage. Due to the limited control of the synthesis, the growth mechanism is still

not clear and to be elucidated. However, the current results strongly suggest that the high reaction pressure is considerably important to the formation of larger {001} surface. The crystal structure was also measured using X-ray diffraction (XRD, Figure 8D). All three samples displayed similar crystallinity and the same crystal structure that belonged to the $I-42m$ space group.^[7] Although the uniformity of those samples needed to be improved as indicated in the SEM images, our comparative study on the crystallinity of the three samples with the continuous increment of the intensity-ratio of 002 and 101 peaks (normalized according to 002 diffraction), provided another evidence on the enlargement of {001} surface.^[12a]

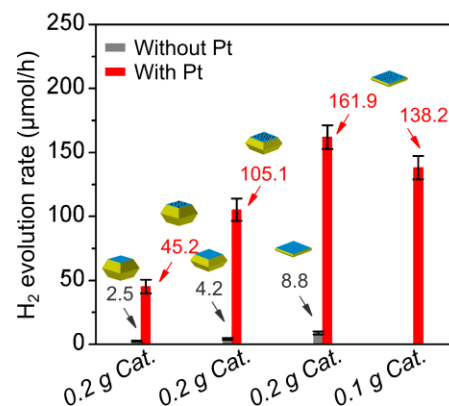


Figure 9. Visible-light-driven hydrogen production rates with or without Pt (0.5 wt%) co-catalyst for 5-h test over the as-prepared decahedra with small, moderate, and large {001} facets. Photocatalytic reaction condition: Catalyst: 0.2 g, 180 mL aqueous solution containing 0.35 M Na_2S and 0.25 M Na_2SO_3 , side irradiation Pyrex cell, cutoff filter ($\lambda \geq 430$ nm), CHF-XM500 Xe lamp. Error bars are standard errors of three tests ($n = 3$).

Finally, we examined the photocatalytic performance of the as-prepared Cu_2WS_4 decahedral photocatalysts to study the effect taken by the separated reaction sites, as well as the changes on the ratio of {001}/{101} facets. As shown in Figure 9, without the presence of noble metal co-catalyst, only a small amount of hydrogen was detected. However, the decahedra with larger {001}/{101}-ratio showed improved photocatalytic H_2 evolution rate. Together with electron-inductive behavior of {001} facets, it is believed that the half reaction, namely photoreduction reaction should act as the kinetically determining step during the hole-scavenger contained photocatalytic procedure. More importantly, after 0.5 wt% Pt was in-situ deposited, hydrogen evolution rates for all samples was further improved *ca.* 20 times, which is ascribed to the synergistic effect of selective Pt-deposition on {001} facets and the reduction nature of {001} surface.^[5a] On the other hand, the significant improvement reveals the great distinction between the rates of photoinduced reduction and oxidation, indicating that very few oxidation sites are required in the reaction.

To evaluate the effect of surface area for this reaction, we firstly measured the surface area of the samples, with 1.501 m²/g, 2.103 m²/g, and 3.372 m²/g for the decahedra of smallest, larger, and biggest {001}/{101} ratios, respectively. Interestingly, using 0.1 g photocatalyst shown in Figure 8C, the hydrogen evolution rate is 138.2 μmol/h (Figure 9), which is about 3 times of the smallest-{001} decahedra shown in Figure 8A (while the total surface areas of the two samples are nearly the same). It is therefore believed that, compared to the surface area, the change of {001}/{101} should play a more important role to the photoreactivity. In addition, time-coursed hydrogen production test was also carried out using Cu₂WS₄ decahedral photocatalysts synthesized via a surfactant(PVP)-assisted hydrothermal method. The result was shown in Figure S5. Clearly, no notable deactivation for hydrogen production was observed. The well maintained stability of the reaction for over 20 hours indicates the negligible impact of residual PVP in the sample. Significantly, SEM image of the recovered samples implies the reaction is indeed photocatalytically proceeded (Figure S6). Taken all, we believe that facet engineering offers a novel approach to qualitatively or even quantitatively studying the kinetics of a given photocatalytic reaction.

It is worth pointing out that we also tried to measure the photocatalytic oxidation activity of {101} facets by using IO₃⁻, AgNO₃, and K₂S₂O₈ as electron scavengers, respectively. However, no oxidation products, e.g., O₂, was detected. It is considered that for chalcogenide photocatalyst, photoinduced self-corrosion occurred rather than oxidation of OH⁻. Despite of this, we still expect the development of a method to the evaluation of the oxidation abilities of shaped chalcogenide photocatalysts.

Conclusion

In summary, we have shown, for the first time, photoinduced oxidative etching could indicate the photooxidation reaction sites of chalcogenide photocatalyst. The investigation relies on the use of single-crystal Cu₂WS₄ decahedral photocatalysts and the observation of separated metal deposition and oxidative etching over {001} and {101} facets caused by photoinduced reduction and oxidation, respectively. Significantly, with the well adjusted reaction active sites according to the reaction kinetics, i.e., the ratio of {001}/{101} facets, photocatalytic activity could be further enhanced. Our work thus provides a facile way to judge the redox reaction sites of chalcogenide photocatalysts and enhancing their activity by surface-facet engineering. We believe the use of etching provides a new approach to revealing the photocatalytic oxidation reactions over certain crystal facets, towards which, one can rationally design and fabricate a given chalcogenide photocatalyst with desired crystallinity in terms of both stability and activity.

Acknowledgements

This work was supported by the National Nature Science Foundation of China (No. 51236007, No. 51121092, No.

31070517), 863 Program of Department of Sciences and Technology of China (No.2012AA051501), the National Basic Research Program of China (973 Program, No. 2013CB932902). We also appreciate the assistance of B. Wang and P. Guo, and thank Dr D. Jing and Dr J. Shi for helpful discussions and critical reading of the manuscript.

Notes and references

^a Prof. J. Zhou, Prof. Y. Sun, N. Li

School of Chemistry and Chemical Engineering
Southeast University, Nanjing, Jiangsu, 211189 (P. R. China)
E-mail: jczhou@seu.edu.cn

^b Prof. L. Guo, Dr. M. Liu, Dr. Z. Zhou

International Research Center for Renewable Energy
State Key Laboratory of Multiphase Flow
Xi'an Jiaotong University, Xi'an, Shaanxi 710049 (P. R. China)
E-mail: lj-guo@mail.xjtu.edu.cn

† These authors contributed equally to this work.

Electronic Supplementary Information (ESI) available: XRD pattern, UV-vis spectrum, partial density of states (DOS) of S, W, and Cu on the (A-C) {001} and (E-F) {101} facets, TEM image viewed from [010] direction, and corresponding selected-area electron diffraction (SAED) pattern of Cu₂WS₄ photocatalyst. High-resolution XPS spectra of Pt and Ru of 5 wt% Pt/Cu₂WS₄ and 5 wt% Ru/Cu₂WS₄ photocatalysts. Time-coursed photocatalytic hydrogen production over Cu₂WS₄ decahedra with biggest {001} facets, and SEM image of recovered Pt-Cu₂WS₄ sample after the photocatalytic reaction.

See DOI: 10.1039/b000000x/

- 1 a) A. J. Bard, M. A. Fox, *Acc. Chem. Res.* **1995**, *28*, 141-145; b) X. Chen, S. Shen, J. Guo, S. Mao, *Chem. Rev.* **2010**, *110*, 6503-6570; c) M. Gratzel, *Nature* **2001**, *414*, 338-344; d) Y. D. Hou, B. L. Abrams, P. C. K. Vesborg, M. E. Björketun, K. Herbst, L. Bech, A. M. Setti, C. D. Damsgaard, T. Pedersen, O. Hansen, J. Rossmeisl, S. Dahl, J. K. Nørskov, I. Chorkendorff, *Nature Mater.* **2011**, *10*, 434-438; e) A. Kudo, Y. Miseki, *Chem. Soc. Rev.* **2009**, *38*, 253-278; f) N. S. Lewis, D. G. Nocera, *Proc. Natl. Acad. Sci. USA* **2006**, *103*, 15729-15735; g) Y. Tachibana, L. Vayssieres, J. R. Durrant, *Nature. Photon.* **2012**, *6*, 511-518; h) D. Jing, L. Jing, H. Liu, S. Yao, L. Guo, *Ind. Eng. Chem. Res.* **2013**, *52*, 1982-1991.
- 2 A. Fujishima, K. Honda, *Nature* **1972**, *238*, 37-38.
- 3 a) N. Buhler, K. Meier, J. F. Reber, *J. Phys. Chem.* **1984**, *88*, 3261-3268; b) I. Tsuji, H. Kato, A. Kudo, *Angew. Chem. Int. Ed.* **2005**, *44*, 3565-3568; c) M. Liu, D. Jing, Z. Zhou, L. Guo, *Nat. Commun.* **2013**, *4*, 3278; d) M. Liu, L. Wang, G. Lu, X. Yao, L. Guo, *Energy Environ. Sci.* **2011**, *4*, 1372-1378; e) H. Kato, K. Asakura, A. Kudo, *J. Am. Chem. Soc.* **2003**, *125*, 3082-3089; f) J. H. Park, S. Kim, A. J. Bard, *Nano Lett.* **2005**, *6*, 24-28; g) Z. G. Zou, J. H. Ye, K. Sayama, H. Arakawa, *Nature* **2001**, *414*, 625-627; h) X. C. Wang, K. Maeda, A. Thomas, K. Takanabe, G. Xin, J. M. Carlsson, K. Domen, M. Antonietti, *Nature Mater.* **2009**, *8*, 76-80; i) K. Maeda, K. Teramura, D. Lu, T. Takata, N. Saito, Y. Inoue, K. Domen, *Nature* **2006**, *440*, 295; j) K. Maeda, T. Takata, M. Hara, N. Saito, Y. Inoue, H. Kobayashi, K. Domen, *J. Am. Chem. Soc.* **2005**, *127*, 8286-8287; k) X. Xu, C. Random, P. Efsthathiou, J. T. S. Irvine,

- Nature Mater.* **2012**, *11*, 595-598; l) X. B. Chen, L. Liu, P. Y. Yu, S. S. Mao, *Science* **2011**, *331*, 746-750.
- 4 a) X. Wang, Q. Xu, M. Li, S. Shen, X. Wang, Y. Wang, Z. Feng, J. Shi, H. Han, C. Li, *Angew. Chem. Int. Ed.* **2012**, *51*, 13089-13092; b) J. Zhang, Q. Xu, Z. Feng, M. Li, C. Li, *Angew. Chem. Int. Ed.* **2008**, *47*, 1766-1769; c) Q. Xiang, J. Yu, M. Jaroniec, *J. Am. Chem. Soc.* **2012**, *134*, 6575-6578; d) J. Zhang, J. Yu, Y. Zhang, Q. Li, J. R. Gong, *Nano Lett.* **2011**, *11*, 4774-4779; e) M. T. Mayer, Y. Lin, G. Yuan, D. Wang, *Acc. Chem. Res.* **2013**, *46*, 1558-1566; f) H. Tada, T. Mitsui, T. Kiyonaga, T. Akita, K. Tanaka, *Nature Mater.* **2006**, *5*, 782-786; g) Ariando; X. Wang, G. Baskaran, Z. Q. Liu, J. Huijben, J. B. Yi, A. Annadi, A. R. Barman, A. Rusydi, S. Dhar, Y. P. Feng, J. Ding, H. Hilgenkamp, T. Venkatesan, *Nat. Commun.* **2011**, *2*, 188; h) H. G. Kim, P. H. Borse, W. Choi, J. S. Lee, *Angew. Chem. Int. Ed.* **2005**, *44*, 4585-4589.
- 5 a) R. Li, F. Zhang, D. Wang, J. Yang, M. Li, J. Zhu, X. Zhou, H. Han, C. Li, *Nat. Commun.* **2013**, *4*, 1432; b) H. G. Yang, C. H. Sun, S. Z. Qiao, J. Zou, G. Liu, S. C. Smith, H. M. Cheng, G. Q. Lu, *Nature* **2008**, *453*, 638-641; c) G. Liu, J. C. Yu, G. Q. Lu, H. M. Cheng, *Chem. Commun.* **2011**, *47*, 6763-6783; d) T. Ohno, K. Sarukawa, M. Matsumura, *New J. Chem.* **2002**, *26*, 1167-1170; e) J. Pan, G. Liu, G. Lu, H. M. Cheng, *Angew. Chem. Int. Ed.* **2011**, *50*, 2133-2137; f) T. Tachikawa, S. Yamashita, T. Majima, *J. Am. Chem. Soc.* **2011**, *133*, 7197-7204; g) C. G. Read, E. M. P. Steinmiller, K. S. Choi, *J. Am. Chem. Soc.* **2009**, *131*, 12040-12041.
- 6 a) A. Selloni, *Nature Mater.* **2008**, *7*, 613-615; b) J. Zhu, S. Wang, Z. Bian, S. Xie, C. Cai, J. Wang, H. Yang, H. Li, *CrystEngComm* **2010**, *12*, 2219-2224; c) X. H. Yang, Z. Li, G. Liu, J. Xing, C. Sun, Li, C. Yang, *CrystEngComm* **2011**, *13*, 1378-1383.
- 7 D. Jing, M. Liu, Q. Chen, L. Guo, *Int. J. Hydrogen Energy* **2010**, *35*, 8521.
- 8 a) Z. Zheng, B. Huang, J. Lu, X. Qin, X. Zhang, Y. Dai, *Chem. Eur. J.* **2011**, *17*, 15032-15038; b) P. M. Oliver, G. W. Watson, E. T. Kelsey, S. C. Parker, *J. Mater. Chem.* **1997**, *7*, 563-568; c) Z. K. Zheng, B. B. Huang, Z. Y. Wang, M. Guo, X. Y. Qin, X. Y. Zhang, P. Wang, Y. Dai, *J. Phys. Chem. C* **2009**, *113*, 14448-14453; d) D. Wang, P. Kanhere, M. Li, Q. Tay, Y. Tang, Y. Huang, T. C. Sum, N. Mathews, T. Sritharan, Z. Chen, *J. Phys. Chem. C* **2013**, *117*, 22894-22902.
- 9 J. Yang, D. Wang, H. Han, C. Li, *Acc. Chem. Res.* **2013**, *46*, 1900-1909.
- 10 Y. Miseki, H. Kato, A. Kudo, *Energy Environ. Sci.* **2009**, *2*, 306-314.
- 11 a) C. D. Wagner, *Handbook of x-ray photoelectron spectroscopy: a reference book of standard data for use in x-ray photoelectron spectroscopy*, Physical Electronics Division, Perkin-Elmer Corp., **1979**; b) D. Perry, J. A. Taylor, *J. Mater. Sci. Lett.* **1986**, *5*, 384-386; c) V. G. Bhide, S. Salkalachen, A. C. Rastog, C. N. R. Rao, M. S. Hegde, *J. Phys. D: Appl. Phys.* **1981**, *14*, 1647-1656; d) B. R. Strohmeier, D. E. Levden, R. S. Field, D. M. Hercules, *J. Catal.* **1985**, *94*, 514-530.
- 12 a) D. Wang, H. Jiang, X. Zong, Q. Xu, Y. Ma, G. Li, C. Li, *Chem. Eur. J.* **2011**, *17*, 1275-1282; b) Y. Xia, Y. Xiong, B. Lim, S. E. Skrabalak, *Angew. Chem. Int. Ed.* **2009**, *48*, 60-103; c) M. Jin, H. Zhang, Z. Xie, Y. Xia, *Energy Environ. Sci.* **2012**, *5*, 6352-6357.